The role of strain-induced passivity breakdown in corrosion crack initiation

Andrey P. Jivkov*

Solid Mechanics, Malmö University, 205 06 Malmö, Sweden.

Abstract

Corrosion crack nucleation and growth are modelled as a moving boundary problem. The model incorporates three physical processes – dissolution, passivation and straining – into a continuum mechanical framework. The dissolution triggers surface advance; the passivation restrains the access of the environment to bare metal; the deformation causes for passivity breakdown. Plane cracks nucleating from surface pits in an elastic-plastic material body under fatigue load are considered. The problem is solved using a FEM program and a moving boundary tracking procedure. The model simulates how cracks form and grow in a single continuous course. The geometry of the developed cracks is found independent of the initial pit size. Plasticity is found to influence the curvature at the tip of the nucleated corrosion cracks. The most important evolution length parameter, the width of the corrosion crack, is found to depend on the size constraints of the tracking procedure. It is concluded that the model is deficient for determining all length scales observed in reality. Physical processes to be considered in an advanced model are proposed and discussed.

Keywords: Stress-corrosion cracking; Crack evolution; Moving boundary; Finite elements; Crack geometry.

1. Introduction

Stress-corrosion cracking (SCC) has been a subject of intense research during the last three decades. The standpoint in this research is that aggressive environments introduce corrosion, which in synergy with the mechanical load further deteriorates the material and shortens the life of structural members. Corrosion is a complex phenomenon, which broadly speaking includes dissolution, i.e. passage of metal atoms from the solid surface to the environment; and passivation, i.e. formation of a protective layer of corrosion products on the surface that guards it against further dissolution. In most structural materials the formed layer, called also passive film, is several nanometers thin but sufficient to decrease the rate of dissolution several orders of magnitude. A widely used hypothesis for the mechanism of SCC is that the crack advances due to localised dissolution [1,2]. The role of the mechanical loading is thought of as damaging the film in the surface region with highest strains, thus exposing bare metal for dissolution. The passivation process continuously restores the ruptured film. Hence, the interaction between the loading and the passivation defines the balance necessary for strain and dissolution localisation in the crack tip region, which maintains the shape of the evolving crack. Recent experimental studies have shown that active loading is an essential prerequisite for continuing corrosion cracking, which is a strong support for the key role of the deformation-film interaction [3,4].

Mechanistic models for SCC based on localised dissolution hypothesis assume corrosion crack growth, where a single parameter such as the crack tip opening

* Tel: +46-40-6657626; Fax: +46-40-6657135; E-mail: andrey.jivkov@ts.mah.se

displacement, or the stress intensity factor is determining all the features from a solid mechanics perspective [5,6]. This means that from such a perspective, the crack possesses geometry with atomically sharp tip, and formulating a crack growth criterion reflecting the mechanism of dissolution-governed crack advance becomes a difficult task. The corrosion cracks observed in reality, however, do not have atomically sharp tips, but rather look like long slender notches (Fig. 1). Hence, they possess intrinsic length parameters like the crack width and the radius of curvature at the tip. A simple model for strain-driven corrosion growth of cracks with such realistic geometries has been recently proposed in [7]. The results have demonstrated that the local geometry at the tip strongly affects the corrosion crack growth rate. This means that the single parameter description of the mechanistic models [5,6] could not be completely adequate in predicting SCC growth rates. The questions arising here are what in reality determines the crack tip geometry and is the balance between deformation and passivation a sufficient condition to maintain this geometry. These questions might be answered by turning our attention to the stage of crack initiation. Existence of corrosion pits is considered to be a major source for corrosion crack initiation [8,9]. The strain-driven dissolution model from [7] was used in the work [10] to pose a problem for crack nucleation from surface pits. The study reported in [10], however, considered an elastic material behaviour and emphasised on the influence of the initial pit geometry on the nucleation time and crack extension. This work could not answer the questions asked here, because there was effectively only one physical length scale introduced into the problem via the size (width) of the existing surface pit.

To establish a new length scale, the present study considers elastic-plastic materials. The model for strain-driven dissolution from [7] and the moving boundary value problem posed in [10] are used and therefore briefly described in section 2. The numerical solution to the problem is discussed in section 3 in some more detail, since it is found important for the results, discussion and conclusions.

2. Problem with surface evolution model

The geometry of the studied problem is illustrated in Fig. 2. A plane body occupying the region $0 \le X_1 \le B$ and $|X_2| \le B$ with respect to a fixed coordinate system (X_1, X_2) is considered (Fig. 2a). A shallow surface pit of width $W = 10^{-3}B$ and depth $D = 10^{-4}B$ is introduced in the vicinity of the coordinate system origin (Fig. 2b). The material of the body is chosen elastic-perfectly plastic with modulus of elasticity E = 206 GPa, Poisson's ratio ν = 0.3, and yield strength σ_y. The body is considered to be in plane strain. The load is applied in cycles via prescribed displacements. For simplicity, the cycles are taken of rectangular shape with period T and displacement magnitude u. If the components of the displacement and the traction vectors are denoted by U_1, U_2, and T_1, T_2, respectively, the boundary conditions of the quasi-static problem of one cycle are

$$T_1 = T_2 = 0, \quad \text{along} \quad X_1 = 0 \,(\text{including pit surface}), \tag{1a}$$

$$T_1 = 0 \quad \text{and} \quad U_2 = -u, \quad \text{along} \quad X_2 = -B, \tag{1b}$$

$$U_1 = T_2 = 0, \quad \text{along} \quad X_1 = B, \tag{1c}$$

$$T_1 = 0 \quad \text{and} \quad U_2 = u, \quad \text{along} \quad X_2 = B. \tag{1d}$$

The surface $X_1 = 0, |X_2| \le B$ and the pit are assumed to be in contact with a corrosive environment and to be compactly covered by a passive film, i.e. metal dissolution and hence surface evolution is initially prohibited. The film is assumed to have the same mechanical properties as the bulk material of the body both in compression and in tension up to a characteristic strain level – the rupture strain of the film, ε_f. This brittleness under tensile strains is justified by the metal-oxide composition of the passive films. The film thickness does not enter the formulation. A segment of the film-covered solid surface is illustrated in Fig. 3, where dS and ds are the lengths of a differential surface element before and after a mechanical deformation, respectively. This deformation is measured by the strain parallel to the surface, $\varepsilon = (\mathrm{d}s - \mathrm{d}S) / \mathrm{d}s$. Upon load application during one load cycle the film deforms together with the bulk. If the strain at a number of surface points reaches the rupture strain, ε_f, the film breaks at these points and a corresponding number of film fragments separated by gaps of bare metal are created. The film fragments are then supposed to fully relax. The unprotected gaps are exposed to the corrosive environment and the metal dissolves, advancing that portion of the surface. The dissolution occurs normally to the surface. The rate of the dissolution process depends on the simultaneously operating repassivation process. In a short time the latter restores the film properties of an intact film, i.e. interrupts the active dissolution. The repassivation time may vary from a few seconds to a few minutes, depending on the solid-environment composition. The time dimension of the problem, however, is not of interest in this work. Therefore, the cycle period of the fatigue load, T, is assumed to be sufficiently large to allow full restoration of the film before the next cycle is applied. The advance per load cycle in every gap formed along the film-covered surface is assumed constant, denoted by R_d in Fig. 3. This assumption is quite rough from an electrochemical perspective and the possible consequences will be conferred in the discussion section.

A continuum surface advance may be determined by "smearing" the advances in the gaps over the deformed length of the differential element, as shown in Fig. 3, $R = R_d\, \varepsilon$. Then, the advance of a surface point during one load cycle is suggested proportional to the surface strain, ε, via

$$R = R_d\, \varepsilon\, \theta\left(\varepsilon - \varepsilon_f\right), \tag{2}$$

where $\theta(x)$ is the Heaviside step function, i.e. $\theta(x) = 1$ if $x > 0$, and $\theta(x) = 0$ otherwise. The Heaviside step function introduced in Eq. (2) reflects the assumption that no dissolution is allowed in the surface points with intact passive film. Note, that Eq. (2) represents an additional to Eq. (1a) boundary condition along the contact surface $X_1 = 0$, including the pit surface.

The rupture strain of the passive film is chosen as $\varepsilon_f = 0.001$ for the calculations and the magnitude of the applied displacements is chosen as $u = \varepsilon_f B$. This choice ensures a constant strain field in a rectangular body without surface flaw, which is exactly on the threshold to break the protective film of the flat surface. Any small deviation from a flat surface, however, will create sufficient strain concentration to break the film and start the process of strain-driven corrosion.

3. Solution with moving boundary refinement

The geometry, the material model and the boundary conditions (1) and (2) from the previous section constitute a moving boundary value problem (MBVP), where each load cycle is understood as a new boundary value problem. The new problem geometry is determined by the entire past history of the evolving boundary. The equilibrium solution for the new problem defines the present evolution. The numerical solution for the MBVP, proposed here, is based on a problem split into equilibrium and evolution parts over each load cycle. The equilibrium part is solved using a commercial finite element analysis program [11]. Constant strain triangular finite elements are used in the analysis. The surface strains, ε, obtained at equilibrium, provide the advance of the corroding surface via Eq. (2).

In the finite element environment, the surface advance is represented by surface node displacements. In order to properly follow the surface shape changes, a new distribution of nodes along the evolved surface is essential. The existing nodes along the evolving surface at the beginning of a load cycle, define via Eq. (2) the positions of the same number of points along the advanced surface at the end of the load cycle. A B-spline curve is created along the new surface using these points as spline knots [12]. The nodes along that curve are distributed using a surface refinement process, based on one curvature and two length constraints. At every step of the surface refinement process, the nodes already introduced form a polygon of line segments. The curvature constraint is given by the maximum angle, $\delta_{\max}$ that two neighbouring segments are allowed to make. The length constraints specify the maximum and the minimum allowed node spacing and are denoted by $d_{\max}$ and $d_{\min}$, respectively. The maximum node spacing is used to initially distribute nodes along the B-spline at regular distances. After this initial meshing, the refinement procedure is based on segment splitting using the maximum angle and minimum distance constraints.

Fig. 4 illustrates the refinement of a segment s_i, enclosed between the existing nodes, n_i and n_{i+1}. The curve described by the B-spline is shown with a dotted line while the existing line segments are drawn with full lines. Firstly, the length of the current segment, denoted by d_i, is checked against the minimum node spacing. If $d_i < 2\, d_{\min}$ the segment is accepted as not requiring further refinement. Otherwise, the position of the point along the B-spline, lying midway between n_i and n_{i+1} is calculated. This point is shown with an unfilled circle in the figure. The two potential segments, connecting the introduced point with the existing nodes are shown with dashed lines. The oriented angle between them is denoted by δ_i. If $\delta_i < \delta_{\max}$ the current segment does not require further refinement, since the curvature criterion is met. If $\delta_i \geq \delta_{\max}$ the unfilled point is introduced as a new node along the surface, and the dashed segments become newly accepted parts of the boundary polygon. The procedure runs over all currently existing line segments and terminates when there are no more segments, requiring refinement.

After displacing the corroding surface to its evolved position the current geometry is changed. The interior of the evolved body is re-meshed using a Delauney-type triangulation procedure [13]. The residual stresses and plastic strains, obtained after a load cycle closing, have been neglected when defining the boundary value problem for the next cycle. This was done for the sake of computational efficiency. Tests with re-mapping of stresses and plastic strains onto the new configuration were performed and

while the computational time increased dramatically, the results were found to differ irrelevantly from those with neglected residual fields.

4. Results

Two different types of simulations have been performed – variable yield strength and variable constraints of boundary refinement procedure. During all numerical simulations the condition $d_{max} = 10\, d_{min}$ has been maintained. A normalised load factor, σ_∞ / σ_y, is introduced, where for the given boundary conditions the remotely applied stress is $\sigma_\infty = E\varepsilon_f$.

Initially, a number of yield strengths in the interval $0 \le \sigma_\infty / \sigma_y \le 0.5$ have been tested with fixed constraints $d_{min} = 5\times10^{-3}W$ and $\tan(\delta_{max}) = 0.15$. Note that, for edge cracks, the load interval $\sigma_\infty / \sigma_y < 0.32$ defines small scale yielding (SSY) conditions according to ASTM convention. A typical crack evolution obtained with the parameters $d_{min} = 5\times10^{-3}W$, $\tan(\delta_{max}) = 0.15$ and $\sigma_\infty / \sigma_y = 0.25$ is shown in Fig. 5. The profiles of the initial pit, the surface at crack incubation, and the crack at extension W are presented. The current crack length is denoted by a. The crack width in the tip region, 2ρ, is defined as the distance between the points where 45° lines running back from the crack tip intercept the crack faces.

The crack width attained at incubation was found to be independent of the material yield strength and of the initial pit geometry. To show the latter statement, two series of simulation have been performed. Firstly, minimal element sizes in the interval $10^{-3} \le d_{min} / W \le 10^{-2}$ have been tested with fixed values $\sigma_\infty / \sigma_y = 0.25$ and $\tan(\delta_{max}) = 0.15$. Secondly, simulations for a number of maximal angles in the interval $0.07 \le \tan(\delta_{max}) \le 0.21$ have been performed with the parameters $\sigma_\infty / \sigma_y = 0.25$ and $d_{min} = 2\times10^{-3}W$. Fig. 6 shows the results of these two simulation series – ρ vs. d_{min} (a) and ρ vs. δ_{max} (b). The attained incubation crack width was found to be $2\rho \approx 10 d_{min}$. For sufficiently small δ_{max}, the crack width becomes independent of that constraint, for example for $\delta_{max} < 9°$ when $d_{min} = 2\times10^{-3}W$. The same independence of the initial geometry and material yield strength was found for crack extension at incubation, $a_{inc} \approx 10\rho$ as depicted in Fig. 5 and also demonstrated in the next Fig. 7.

Fig. 7 shows the normalised crack growth rate, $(R / R_d)_{tip} = \varepsilon_{tip}$, as a function of the square root of the normalised crack extension, a / W, for three chosen material yield strengths with $\sigma_\infty/\sigma_y = 0$, 0.15, 0.3. The corrosion crack of Fig. 5 has a shape of a deep slender notch. For such a notch with a circular tip region elastic solutions for the stress and strain fields can be found in the literature, e.g. [14]. If the radius at the tip is ρ, the maximum strain at the tip is given by:

$$\varepsilon_{tip} = \frac{2K_I}{E\sqrt{\pi\rho}}, \tag{3}$$

where K_I is the stress intensity factor for a crack of same length as the notch. For edge cracks $K_I \approx 1.1215\sigma_\infty\sqrt{\pi a}$, where $\sigma_\infty = E\varepsilon_f$ in the present study. With a steady value of ρ during crack propagation, proportionality between $\sqrt{a}$, and strain at the tip, ε_{tip}, reveals the existence of a K_I -controlled zone surrounding the tip. This helps to define the crack

incubation point as the onset of a linear relation between crack growth rate and square root of crack extension, Fig. 7. This is also the point where the evolving pit surface attains the width 2ρ.

At the same time, the crack growth rate at and after incubation shows strong dependence on the material yield strength. This suggests that shape changes of the crack tip region have occurred. To demonstrate the extent of these changes an appropriate shape factor is defined using Eq. (3) and the expression for the stress intensity factor as

$$\phi = \frac{(R/R_d)}{2.243\varepsilon_f}\sqrt{\frac{\rho}{a}}\,. \tag{4}$$

The dependence of the shape factor on the yield strength is presented in Fig. 8. Note from Eqs. (3) and (4), that ϕ = 1 if the notch has exactly circular tip shape and the material is elastic. Note also that for a given yield strength, ϕ is proportional to the slope of the corresponding line in Fig. 7, representing crack propagation stage.

If the crack growth illustrated in Figs. 5 and 7 is followed for sufficiently long time, the interaction between the corrosion and the large plastic deformations cause blunting of the tip region. This blunting continues until the crack tip region attains a shape that is maintained self-similar in the continuation of the propagation. The self-similar growth is characterised by an approximately constant rate. The overall growth rate behaviour is illustrated in Fig. 9 for material with σ_∞/σ_y = 0.2. For all cases of elastic-perfectly plastic materials studied here, the onset of blunting was found to be approximately determined by the relation (a / ρ) ($\sigma_\infty^2/E\sigma_y$) = 0.025. If short crack growth is defined as the K_I-controlled stage, i.e. where growth rate is proportional to square root of crack length, then the extend of this growth is depending both on the material yield strength and on the local geometry via the corrosion crack width. In terms of crack opening displacement, δ, for a corresponding ideal crack in a respective material, this relation translates to $\delta \approx 0.05\rho$.

5. Discussion

The model used in this study, as well as in the works [7,10], accounts for three basic processes operating on the solid-environment interface, namely metal dissolution, passive film formation and surface deformation. The dissolution is regarded as a driving process for surface advance. The passivation is a mechanism controlling the contact of bare metal with the corrosive environment. The mechanical deformation of the surface is considered solely as a means for passivity breakdown. A moving boundary value problem is formulated to implement the model with geometry, suitable for studying crack nucleation from surface pits. It is clear from the model description, that the three processes cannot introduce a length parameter into the posed problem. The only length scale is initially established by the width of the existing surface pit. The geometry of the formed corrosion crack in an elastic material, however, was found independent of this length scale. In the present study the moving boundary value problem from [10] has been extended to materials with elastic-plastic material behaviour. The idea was to introduce a new length scale via the size of the plastic zone, developing at the tip of the advancing crack. The results show, that the formed crack width remains independent of

the material yield strength, while the curvature at the crack tip increases with decreasing yield strength (Fig. 8). This leads to enhanced corrosion crack propagation for softer materials.

Three stages of corrosion crack evolution are observed in Fig. 9. The approximately linear relation between crack growth rate and square root of crack extension shows that the stress and strain fields surrounding the crack tip are K_I-controlled. The interval under K_I-control is called short crack growth. The incubation stage is then defined as preceding the short crack growth. During incubation, localisation of strains and dissolution at the tip occur leading to the fully formed crack. A stage, characterised by large deformations in the tip region succeeds the short crack growth. In this non-linear regime, crack tip blunting and self-similar growth are then observed. The major parameter controlling evolution is the crack width, 2ρ. It governs the incubation length and the short crack growth limit via the relations $a_{inc} \approx 10\rho$ and $\delta \approx 0.05\rho$, respectively. The length scale determining the width of the incubated crack, however, is still unsolved.

The proposed numerical solution of the problem is based on a moving boundary tracking procedure, which uses constraints for element size and curvature. These constraints introduce a non-physical length scale, which is found to govern the width of the formed corrosion crack. Fig. 6 suggests that the forming crack tends to minimise its width as much as the numerical constraints allow. This may be considered as a valuable feature of the moving boundary approach, because it leads to corrosion cracks attaining realistic geometrical shapes and allows the study of their evolution. In a limit, however, the observed trend would produce a crack with atomically sharp tip. In reality there must be physical reasons for the established crack width that have not been taken into account in the model.

One possibility is that an additional physical process operating on the solid surface is counteracting the observed tendency for shrinking. A candidate physical process is the diffusion of atoms along the solid surface. The surface diffusion is driven by a gradient of the surface chemical potential and is found to trigger morphology evolution of solid surfaces, e.g. [15,16]. The chemical potential, in the simplest representation, depends on the curvature and the strain energy introduced by external loading. These two factors have opposite effect and their balance determines the wavelength of the evolved surface. Turning back to the nucleation of corrosion cracks, one may expect that this curvature-energy balance is not established, at least not during the incubation stage. While the strain energy density in the region of the nucleating crack has still moderate values, the curvature is increasing dramatically with the trend of the deformation-corrosion interaction to maximise it. This leads to an enhanced diffusion transport of atoms to the area of greatest curvature, i.e. to the forming crack tip. Hence, the interaction between the surface deformation and the dissolution and passivation processes tends to minimise the forming crack width, while the surface diffusion tends to operate in the opposite direction. One may only speculate at present, that the balance between these two tendencies determines the size of the nucleated crack.

Another possibility for improving the model is related to the assumption of a constant penetration advance, R_d (section 2). There are two oversimplifications in this assumption. The first one is that the dissolution rate of the already bare metal does not depend on the local surface state of stress and strain; the latter is used to simply break the protective film. One could expect on physical grounds that the bare surface dissolution rate is altered in a stressed solid. The evidence for that, unfortunately, is

very rarely reported in the literature. The work [17] for example, shows a linear relation between the dissolution rate and the square root of the logarithmic strain. Incorporating this relation into the model, despite of probably making it more realistic, will not solve the problem with the missing length scale.

The second oversimplification is that the dissolution rate is assumed independent of the position along the crack surface and of the local geometry. This is true for a flat freely corroding surface and is nearly true for the initial pit. During the crack formation stage, however, the transport processes in the corrosive environment, e.g. diffusion and electro-migration, lead to a distributed chemistry composition in the cavity, e.g. [18,19]. This yields changes in the electrostatic potential difference between the solid and the environment along the cavity depth, and from there - changes in the dissolution rate. Transport processes become rate determining and also essential for maintaining the conditions needed for dissolution. The idea of how this may help in bringing a length scale is that a decreasing cavity width and an increasing cavity depth may lead to inhibiting the transport processes; most importantly, close to the cavity root. There is no direct support for the former factor influence, because most of the electrochemical studies consider a fixed cavity or crack geometry and deal with one-dimensional transport models. Indirect support for the latter factor could be found in studies of cavities with active walls. For example, it is demonstrated in Ref. [19] that the current density, hence the dissolution rate, decreases from the mouth to the root of a cavity with active walls. In other words, looking back at the evolving crack in Fig. 5, the dissolution rate is lowest at the tip and increases along the active parts of the crack walls until reaching the film-covered surface. In other words, the slower dissolution happens at areas of larger strains (closer to the tip) and the speculation here is that the balance between decreasing dissolution rate, R_d, and increasing strains, ε, along the crack surface will be determining the width of the nucleating crack (see Eq. (2)).

The material microstructure could not be a possible reason for determining the incubation crack with, since the grain boundary (inter-phase) thickness might be a length parameter limiting the crack width from above. The inter-phase thickness, however, may be limiting for the stage of blunting and self-similar growth that the model predicts, Fig. 9.

Regardless of the deficiencies of the used physical model, it is believed that results based on an improved one would show qualitatively the same behaviour of a corrosion crack emerging from a surface pit. To approach a quantitatively predictive model for corrosion crack nucleation, each one of the discussed phenomena must be investigated in a future work.

6. Summary

The model of strain-induced passivity breakdown yields results, which clearly show the importance of the deformation-corrosion interaction for strain and dissolution localisation during crack incubation. This localisation tends to minimise the width of the forming crack. The tendency of vanishing crack width, introduced by the model, is found bounded by the size constraints of the moving boundary tracking procedure. The incubation instance and the subsequent crack evolution are primarily controlled by the nucleated crack width. The crack extension at incubation is found independent of the initial geometry and of the material properties. Plasticity is found to influence the shape

of the crack tip region, but not the crack width. Thus, for softer materials the formed crack tip region is sharper (the curvature at the tip is greater) than for harder materials, which may lead to a crack growth rate increase by about two times. The incubation stage is followed by a K_I-controlled crack growth, the offset of which is also found dependent on the crack width, as well as on the material properties. For larger crack extensions the used model predicts crack tip blunting and self-similar growth under constant rate. The discovered independence of the crack width (and from their the crack growth) from the initial geometry and material constitutive behaviour, yields the necessity of accounting for an additional physical phenomenon (or phenomena), that would introduce the missing length scale. Such phenomena are proposed and have to be considered in an improved model.

Acknowledgments

The financial support of the Swedish Centre for Nuclear Technology (SKC) and the Knowledge Foundation (KKS) is highly appreciated.

References

[1] J.C. Scully. The mechanism of dissolution-controlled cracking. In: P.R. Swann, F.P. Ford, A.R.C. Westwood (Eds.), Mechanisms of Environment Sensitive Cracking of Materials: Proceedings of Metals Society Conference, 1-17, The Metals Society, London (1979).

[2] A. Turnbull. Modelling of environment assisted cracking. Corros. Sci. 34(6), 921-960 (1993).

[3] K. Kussmaul, D. Blind, V. Läpple. New observations on the crack growth rate of low alloy nuclear grade ferritic steels under constant active load in oxygenated high-temperature water. Nucl. Eng. Des. 168(1-3), 53-75 (1997).

[4] J. Heldt, H.P. Seifert. Stress corrosion cracking of low-alloy, reactor-pressure-vessel steels in oxygenated, high-temperature water. Nucl. Eng. Des. 206(1), 57-89 (2001).

[5] F.P. Ford. Quantitative prediction of environmentally assisted cracking. Corrosion 52(5), 375-395 (1996).

[6] G.R. Engelhardt, D.D. Macdonald, M. Urquidi-Macdonald. Development of fast algorithms for estimating stress corrosion crack growth rate. Corros. Sci. 41(12), 2267-2302 (1999).

[7] A.P. Jivkov, P. Ståhle. Strain-driven corrosion crack growth – a pilot study of intergranular stress corrosion cracking. Eng. Fract. Mech. 69(18), 2095-2111 (2002).

[8] Y. Kondo. Prediction of fatigue crack initiation life based on pit growth. Corrosion 45(1), 7-11 (1989).

[9] S.I. Rokhlin, J.Y. Kim, H. Nagy, B. Zoofan. Effect of pitting corrosion on fatigue crack initiation and fatigue life. Eng. Fract. Mech. 62(4-5), 425-444 (1999).

[10] A.P. Jivkov. Evolution of fatigue crack corrosion from surface irregularities. Theor. Appl. Fract. Mech. 40(1), 45-54 (2003).

[11] ABAQUS User's Manual, Version 6.3, Hibbitt, Karlsson & Sorensen Inc. (2002).

[12] G.D. Knott. Interpolating cubic splines. Progress in computer science and applied logic. Birkhauser, Boston (1999).

[13] J.R. Shewchuk. Delaunay refinement algorithms for triangular mesh generation. Comp. Geom. 22(1-3), 21-74 (2002).

[14] H. Tada, P.C. Paris, G.R. Irwin. The stress analysis of cracks handbook, 3d Ed. ASME Press, New York (2000).

[15] D.J. Srolovitz. On the stability of surfaces of stressed solids. Acta Metall. 37(2), 621-625 (1989).

[16] L.B. Freund. Evolution of waviness on the surface of a strained elastic solid due to stress-driven diffusion. Int. J. Solids Struct. 32(6/7), 911-923 (1995).

[17] M.A.V. Devanathan, M.J. Fernando. Kinetics of charge transfer at mechanically strained copper electrodes – I. Anodic dissolution. Electrochim. Acta. 15, 1623-1636 (1970).

[18] S.M. Sharland, Amathematical model of the initiation of crevice corrosion in metals, Corros. Sci. 33(2), 183-201 (1992).
[19] G.R. Engelhardt, M. Urquidi-Macdonald, D.D. Macdonald. A simplified method for estimating corrosion cavity growth rates. Corros. Sci. 39(3), 419-441 (1997).

Figure captions:

Fig. 1. Corrosion crack in a pressure vessel steel component
Fig. 2. Geometry of the boundary value problem
Fig. 3. Strain-film rupture-dissolution model for surface advance
Fig. 4. Step in the surface refinement process
Fig. 5. Crack geometry evolution
Fig. 6. Influence of refinement constraints on incubated crack width
Fig. 7. Crack growth rate behaviour for short extensions
Fig. 8. Crack tip shape factor for variable yield strength
Fig. 9. Extended crack growth rate behaviour

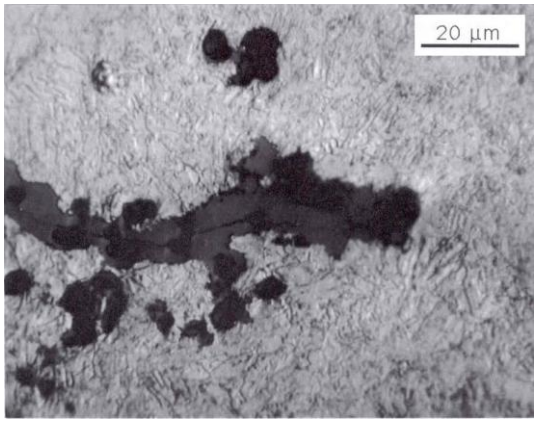

Figure 1. Corrosion crack in a pressure vessel steel component

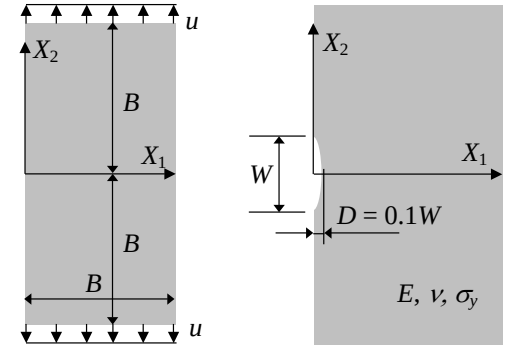

(a) Body geometry (b) Surface pit vicinity

Figure 2. Geometry of the boundary value problem

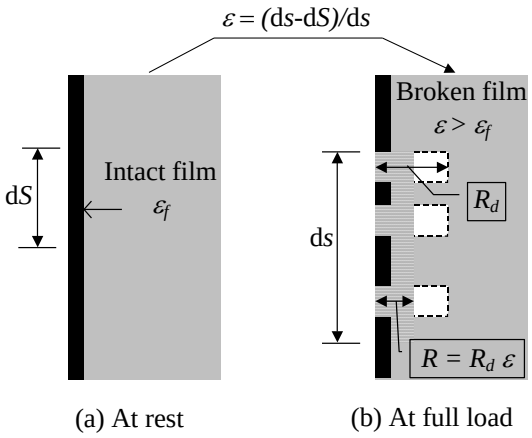

Figure 3. Strain-film rupture-dissolution model for surface advance

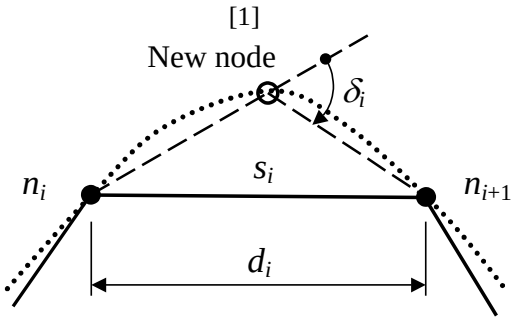

Figure 4. Step in the surface refinement process

[2]

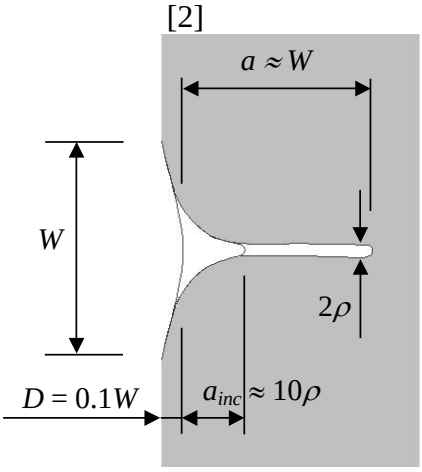

Figure 5. Crack geometry evolution

[3]

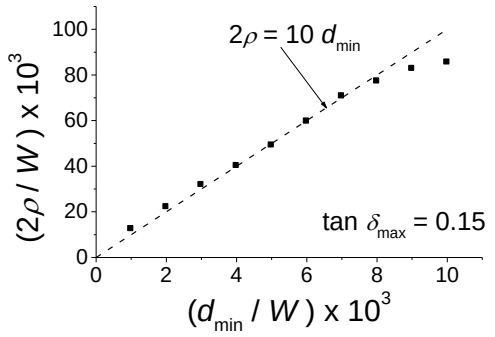

(a) Crack width vs. minimum spacing

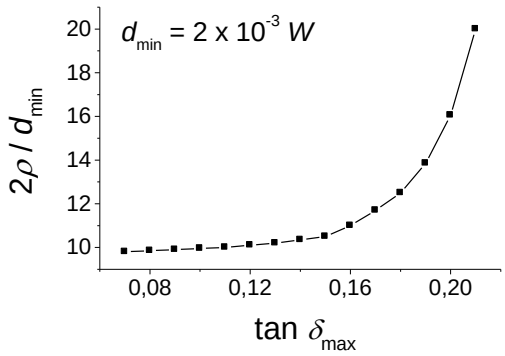

(b) Crack width vs. maximum angle

Figure 6. Influence of refinement constraints on incubated crack width

[4]

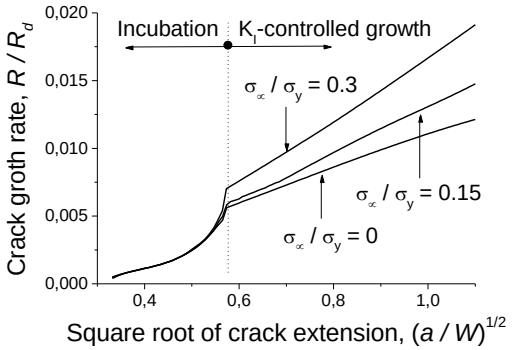

Figure 7. Crack growth rate behaviour for short extensions

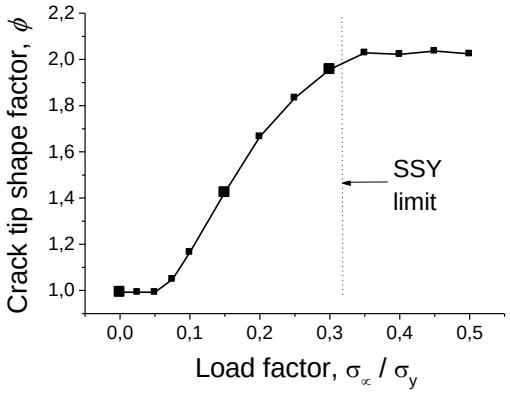

Figure 8. Crack tip shape factor for variable yield strength

[5]

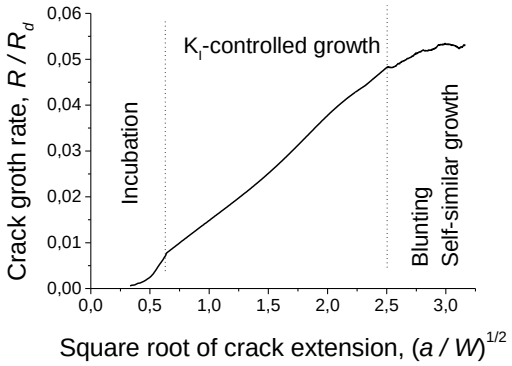

Fig. 9. Extended crack growth rate behaviour